EUROPEAN ORGANISATION FOR NUCLEAR RESEARCH

A Preliminary Measurement of $\mathcal{A}_\tau$ and $\mathcal{A}_\mathrm{e}$ Using 1994 Data

The L3 Collaboration

Abstract

With a data sample of 58,000 $\mathrm{Z} \rightarrow \tau^+\tau^-(\gamma)$ events collected in 1994 we have performed a preliminary measurement of the polarization of τ-leptons as a function of the production polar angle in the barrel region using the following 1-prong τ decay modes: $\tau^- \rightarrow \mathrm{e}^-\overline{\nu}_\mathrm{e}\nu_\tau$, $\tau^- \rightarrow \mu^-\overline{\nu}_\mu\nu_\tau$, $\tau^- \rightarrow \pi^-(\mathrm{K}^-)\nu_\tau$, and $\tau^- \rightarrow \rho^-\nu_\tau$. In addition 38,000 $\mathrm{Z} \rightarrow \tau^+\tau^-(\gamma)$ events collected in 1993 are used for a polarization measurement using the acollinearity in the pion decay mode.

Combining this measurement with our previous measurement, we obtain for the ratio of vector to axial-vector weak neutral couplings for electrons $g_\mathrm{V}^\mathrm{e}/g_\mathrm{A}^\mathrm{e} = 0.0787 \pm 0.0078(\mathrm{stat}) \pm 0.0025(\mathrm{syst})$ and taus $g_\mathrm{V}^\tau/g_\mathrm{A}^\tau = 0.0763 \pm 0.0051(\mathrm{stat}) \pm 0.0044(\mathrm{syst})$ consistent with the hypothesis of $\mathrm{e}-\tau$ universality. Assuming universality of the $e-\tau$ neutral current we determine the effective electroweak mixing angle to be $\sin^2\theta_\mathrm{w}^\mathrm{eff} = 0.2308 \pm 0.0013$.

Submitted to the International Conference on High Energy Physics, Brussels, 27th July through 2nd August 1995

1. Introduction

In the reaction $e^+e^- \to Z \to \tau^+\tau^-$ with unpolarized beams at $\sqrt{s} \approx M_Z$ the final state τ leptons are polarized. This polarization is due to the different couplings of left and right handed leptons to the Z boson. The τ polarization, $\mathcal{P}_\tau(\cos\theta)$, is defined as the asymmetry in the production cross section of τ^- leptons with positive helicity ($h = +1/2$) and negative helicity ($h = -1/2$),

$$\mathcal{P}_{\tau^-}(\cos\theta) = \frac{\sigma(h=+1/2) - \sigma(h=-1/2)}{\sigma(h=+1/2) + \sigma(h=-1/2)}, \tag{1}$$

where θ is the angle between the e^- beam and τ^- flight direction. The τ^- and τ^+ leptons in each event have opposite helicity, so that $\mathcal{P}_{\tau^-}(\cos\theta) = -\mathcal{P}_{\tau^+}(\cos\theta) \equiv \mathcal{P}_\tau(\cos\theta)$. In the improved Born approximation (neglecting radiative corrections, γ-exchange and γZ-interference) $\mathcal{P}_\tau(\cos\theta)$ at the Z pole is given by [1]:

$$\mathcal{P}_\tau(\cos\theta) = -\frac{\mathcal{A}_\tau + 2\mathcal{A}_e\cos\theta/(1+\cos^2\theta)}{1 + 2\mathcal{A}_\tau\mathcal{A}_e\cos\theta/(1+\cos^2\theta)}. \tag{2}$$

The quantities $\mathcal{A}_\ell$ ($\ell = e, \tau$) are defined as $\mathcal{A}_\ell \equiv 2g_V^\ell g_A^\ell/(g_V^{\ell 2} + g_A^{\ell 2})$, where g_V^ℓ and g_A^ℓ denote the effective vector and axial-vector coupling constants. In the framework of the Standard Model [2] the lepton couplings are equal and we use the average of $\mathcal{A}_\tau$ and $\mathcal{A}_e$ to determine the effective electroweak mixing angle through $\mathcal{A}_{e-\tau} \simeq 2(1 - 4\sin^2\theta_w^{eff})$.

In this analysis it is assumed that the decays of the τ are described by a pure V$-$A weak charged current as supported by other measurements [3–7]. The polarization can be derived either from the analysis of the kinematics of single τ decay products [1, 8–10] or from the acollinearity between the decay products of the τ pairs [11]. The following 1-prong τ decay channels have been used in this analysis:

$$\tau^- \to e^-\overline{\nu}_e\nu_\tau \tag{3}$$
$$\tau^- \to \mu^-\overline{\nu}_\mu\nu_\tau \tag{4}$$
$$\tau^- \to \pi^-(K^-)\nu_\tau \tag{5}$$
$$\tau^- \to \rho^-(K^{*-})\nu_\tau \tag{6}$$

where the charge conjugate decays are implied here and throughout this paper. Pions and kaons are not distinguished in the hadronic decay channels.

The analysis of τ polarization described in this paper represents a preliminary result for 1994 data using the barrel region only ($|\cos\theta_{thrust}| < 0.7$). In addition it includes a preliminary measurement from 1993 data using acollinearity in the pion channel. Improvements to these measurement should follow from improvements in the preselection for τ events, the full production of 1994 Monte Carlo, the extension of this study beyond the barrel, a complete study of systematics, and the inclusion of SMD. This measurement, based on a data sample of 58,000 τ pairs taken from a total integrated luminosity of 50pb^{-1}, should be considered preliminary.

2. The L3 detector

The L3 detector is described in detail in reference [15]. The e^+e^- collision point is surrounded by a tracking chamber, a high resolution electromagnetic calorimeter, a cylindrical shell of scintillation counters, a hadron calorimeter and a muon chamber system. The detector is installed in a large magnet providing a uniform 0.5 Tesla field. For the results presented here only the barrel region has been used.

The central tracking chamber consists of a time expansion chamber (TEC) with high spatial resolution in the plane normal to the beam direction surrounded by a Z-Chamber which supplements the $r - \phi$ measurement with a z-coordinate measurement. As shown in figure 1 the transverse momentum resolution of the tracking chamber is $\sigma(1/P_{\mathrm{T}}) = 0.015/\mathrm{GeV}$ in the central region ($|\cos\theta_{TEC}| < 0.7$). The position resolution of a track extrapolated to the electromagnetic calorimeter is 0.2 mm in the plane transverse to the beam direction and 1.5 mm along the beam axis.

The electromagnetic calorimeter is composed of bismuth germanate (BGO) crystals in the shape of truncated pyramids pointing to the interaction region. The BGO barrel has a polar angle coverage of $42^\circ < \theta < 138^\circ$ while the endcaps cover the regions $11.6^\circ < \theta < 38^\circ$ and $142^\circ < \theta < 168.4^\circ$. The energy resolution of the electromagnetic calorimeter for electrons and photons is better than 2% and the position resolution is better than 3 mm above 1.5 GeV.

The hadron calorimeter covers the angular range $5^\circ < \theta < 175^\circ$ and uses depleted uranium absorber plates interleaved with proportional wire chambers oriented alternately along and perpendicular to the beam direction. The readout is grouped into cells in both projections. The energy resolution of the calorimeters for $\pi^\pm$ is $55\%/\sqrt{E(\mathrm{GeV})} + 8\%$.

The muon detector consists of three layers of precise drift chambers which measure the muon trajectory in both the bending and non-bending planes. Muons with polar angle $46^\circ < \theta < 134^\circ$ traverse three layers of drift chambers, and those with angles $37^\circ < \theta < 46^\circ$ and $134^\circ < \theta < 143^\circ$ traverse only two layers. The muon chambers have a momentum resolution of 2.5% for charged particles with $P_{\mathrm{T}} = 45$ GeV traversing three layers of drift chambers.

3. Particle identification

Classification of the τ decay modes is done independently in two hemispheres separated by a plane perpendicular to the thrust axis of the event. Particle identification in each hemisphere is based upon the topological properties of the energy deposition in the electromagnetic and hadron calorimeters with respect to the trajectory of the charged track. This technique is found to be relatively independent of the energy of the τ-decay products, so polarization bias is minimal. In this section we describe the methods used for the identification of one-prong tau decays, whereas the final selection efficiency and the background contamination are discussed in Section 4.

3.1 Preselection

A lepton flavor blind preselection is performed to eliminate $Z \to q\bar{q}$ events. In this preselection, the number of charged tracks observed should be no more than 5 in one hemisphere and 3 in the other. The angle between the thrust axis and the furthest charged track should be less than 30 degrees. In the electromagnetic calorimeter, the number of bumps should not exceed 25. From the most energetic clusters in the calorimeters, the minimum acollinearity and the transverse energy imbalence are calculated. The event is rejected if the acollinearity is greater than 0.45 radian and the energy imbalence is less than 3 GeV.

3.2 Electron identification

Electron candidates consist of an electromagnetic shower in the BGO calorimeter consistent in position and energy with a track in the TEC. The energy deposition in the hadron calorimeter behind this shower must be consistent with the tail of an electromagnetic shower.

The transverse shape of the electromagnetic shower is found to be independent of the electron energy and was defined using $\mathrm{Z} \rightarrow \mathrm{e}^+\mathrm{e}^-(\gamma)$ events. The χ^2 measuring the compatibility of the observed shower with an electromagnetic one is calculated using a 3×3 matrix of BGO crystals around the shower maximum and is required to be less than 30 for 8 degrees of freedom. The angle between the track and the center of gravity of the shower is required to be within 5σ of the detector spatial resolution, corresponding on average to 10 mrad and 20 mrad in the planes perpendicular and parallel to the beam direction respectively. The probability of observing a given track momentum and a given energy in the BGO calorimeter is calculated by maximizing the likelihood for these two measurements to originate from a single electron. A cut on this quantity rejects hadronic τ decays in which a low energy charged track overlaps with a high energy π^0.

3.3 Muon identification

Muons are identified in a redundant way using either information from the muon chambers or from the calorimeters and tracking chamber. In the first approach, a muon candidate consists of a muon chamber track pointing at the interaction point to within 5σ of the spatial resolution of the muon chambers at the interaction point. The second method relies on a track in the tracking chamber matched in space to energy deposition in the hadron calorimeter, and on energy loss in the hadron calorimeter which is consistent with the passage of a muon. The number of hadron calorimeter cells with nonzero energy deposition is required to be at least 50% of all cells along the trajectory of the track. Moreover the energy deposition in the BGO calorimeter must not exceed 1 GeV.

3.4 π^0 identification in hadronic τ decays

An algorithm for finding overlapping neutral and charged energy clusters in the BGO calorimeter is used to determine the number of photons and their energies:

1. The *central* crystal of the shower produced by the charged particle is identified by extrapolating the TEC track to the BGO calorimeter.

2. The energy deposition of the charged particle shower in the BGO calorimeter is estimated by normalizing hadronic shower profile to the energy of the central crystal. The corresponding energy of the charged pion profile is subtracted from the raw energy of each crystal in a 30° half angle cone surrounding the central crystal.

3. All remaining local maxima become photon candidates. The energies and positions of these candidates are defined by fitting the crystal energies with the energy profiles of electromagnetic showers. Single neutral clusters which fit better with the sum of two electromagnetic shower shapes are split.

4. The energies of the neutral shower profiles are then subtracted from the raw BGO crystal energies to obtain an improved estimate of the hadron energy in the central crystal.

Steps 2-4 are iterated, typically three or four times, until all reconstructed particle energies are stable to 1%. At the end the invariant mass of each neutral cluster is estimated by fitting its transverse profile with the sum of two electromagnetic shower shapes. A single neutral cluster forms a π^0 candidate if its energy exceeds 1 GeV and its transverse energy profile is consistent with being electromagnetic or its invariant mass is within 50 MeV of the π^0 mass. Two distinct neutral clusters are considered to form a π^0 candidate if their invariant mass is within 40 MeV of the π^0 mass. The invariant mass of the π^0 candidates is shown in figure 2 for the selected sample of $\tau^- \to \rho^- \nu_\tau$ events.

The sum of energies of reconstructed photons and neutral pions is then subtracted from the total energy in the BGO calorimeter. The remaining energy deposition along with the energy deposition in the hadron calorimeter is assigned to the charged hadron and the estimation of its actual energy is made. This measurement is then combined with the independent measurement of the charged particle momentum in the tracking chamber by maximizing the likelihood for these two measurements to originate from a single hadron. This improves the energy resolution for charged hadrons. The probability corresponding to the maximum of the likelihood function also provides a measure of the compatibility of the track with the energy deposition in the calorimetry.

4. Event selection

The data sample used in this analysis corresponds to an integrated luminosity of 50pb^{-1} collected at $\sqrt{s} \approx M_Z$ in the 1994 LEP run.

The selection of τ decays proceeds in three steps. First, a sample of low multiplicity, back-to-back events is preselected, which consists mainly of leptons from Z decays. This preselection, described in detail in reference [14], suppresses such background as cosmic muons, hadronic Z decays, two-photon and beam-gas interactions. In the second step the individual τ decays are identified. Finally, requirements are placed on the hemisphere opposite to the τ decay candidate in order to suppress the non-τ background.

The final data sample consists of events in which at least one of the τ's decays into one of the 4 channels listed in the introduction. Selection efficiencies are calculated using Monte Carlo simulation of $\mathrm{Z} \to \tau^+\tau^-(\gamma)$ [16] including full simulation of the L3 detector response [1]. However, with 1994 Monte Carlo production still in progress, the Monte Carlo used in this study represents the 1992 and 1993 detector.

The background contamination from non-τ sources like $\mathrm{e}^+\mathrm{e}^-(\gamma)$, $\mu^+\mu^-(\gamma)$, $\mathrm{Z} \to$ hadrons, two photon reactions, cosmics and beam-gas interactions is estimated primarily from the data using either the side opposite to the selected decay or global event characteristics. The corresponding Monte-Carlo for the background simulation [19] was used only to crosscheck these estimates.

The number of selected decays for each channel is listed in Table 1. Below we describe the details of the selection of the individual channels.

4.1 Selection of $\tau^- \to \mathrm{e}^-\overline{\nu}_\mathrm{e}\nu_\tau$

Selection of $\tau^- \to \mathrm{e}^-\overline{\nu}_\mathrm{e}\nu_\tau$ candidates requires an electron candidate in the barrel region of the BGO calorimeter ($|\cos\theta_{\mathrm{thrust}}| < 0.7$). To remove $\mathrm{Z} \to \mathrm{e}^+\mathrm{e}^-(\gamma)$ background, events with two

[1]The L3 detector simulation is based on GEANT Version 3.14; see ref. [17]. The GHEISHA program [18] is used to simulate hadronic interactions.

Table 1: Summary of the number of decays for each channel.

Channel	1990 through 1993 data sample	1994 data sample barrel only	Total
$e^-\bar{\nu}_e\nu_\tau$	13686	11599	25285
$\mu^-\bar{\nu}_\mu\nu_\tau$	14343	10450	24793
$\pi^-\nu_\tau$	11109	8405	19514
$\rho^-\nu_\tau$	21760	16300	38060

identified electrons and total energy deposition in the BGO calorimeter greater than 80% of the center of mass energy are rejected. Events with an electron candidate on the opposite side are also rejected if its energy either exceeds 43 GeV or cannot be reliably measured (due to a dead BGO crystal in the vicinity of the shower maximum), or if the difference between the transverse energies in the two event hemispheres is less than 1 GeV. The last cut removes the small residual background from two-photon interactions left after the preselection.

The selection efficiency for $\tau^- \to e^-\bar{\nu}_e\nu_\tau$ is estimated to be 76% inside the fiducial region and is independent of electron energy above 8 GeV as shown in figure 3. The backgrounds are 1.5% from other τ decays, 1.8% from $Z \to e^+e^-(\gamma)$ and 2.0% from two-photon interactions.

4.2 Selection of $\tau^- \to \mu^-\bar{\nu}_\mu\nu_\tau$

Selection of $\tau^- \to \mu^-\bar{\nu}_\mu\nu_\tau$ candidates requires both identification criteria described in Section 3.3 to be fulfilled in the selected hemisphere. Events with a muon candidate on the opposite side are rejected if either the momentum measured in the muon chambers exceeds 40 GeV, or there is no muon chamber track but the hemisphere contains a muon candidate, or if the difference between the transverse energies in the two event hemispheres is less than 1 GeV. These cuts remove $Z \to \mu^+\mu^-(\gamma)$ background as well as the background from two-photon interactions left after the preselection.

The selection efficiency for $\tau^- \to \mu^-\bar{\nu}_\mu\nu_\tau$ is 70% inside the fiducial region and is independent of the muon momentum above 4 GeV. The background contributions are 1.0% from other τ decays, 7.1% from $Z \to \mu^+\mu^-(\gamma)$, 0.4% from two photon reactions and 0.1% from cosmics.

4.3 Selection of $\tau^- \to \pi^-(K^-)\nu_\tau$

The hemispheres with identified electron or muon candidates are not considered for the selection of the decay mode $\tau^- \to \pi^-(K^-)\nu_\tau$. The decays $\tau^- \to \pi^-(K^-)\nu_\tau$ may contain low energy neutral clusters arising from fluctuations in the hadron shower while the neutral pions in $\tau^- \to \rho^-\nu_\tau$ and $\tau^- \to a_1^-\nu_\tau$ decays give rise to higher energy photon or π^0 candidates. The $\tau^- \to \pi^-(K^-)\nu_\tau$ selection therefore admits no π^0 candidates and no photon candidates with energy greater than 0.5 GeV. The probability that the observed track momentum and calorimetric energy originate from a single hadron is required to exceed 0.003. In order to reject background from $Z \to e^+e^-(\gamma)$ and $Z \to \mu^+\mu^-(\gamma)$, events with an electron or a muon candidate on the opposite side are rejected if its energy exceeds 42 GeV or can not be reliably measured.

The efficiency of $\tau^- \to \pi^-(K^-)\nu_\tau$ selection is 72% in the barrel. The efficiency is relatively independent of the pion energy above 5 GeV as shown in figure 5. The background in the barrel is 11.4% from other τ decays, 0.8% from Bhabha events, 1.7% from two photon interactions 0.3% from dimuon events, and 0.6% from cosmics.

4.4 Selection of $\tau^- \to \rho^- \nu_\tau$

To select an event for the $\tau^- \to \rho^- \nu_\tau$ channel exactly one π^0 candidate is required in the hemisphere. The probability that the measured track momentum and calorimetric energy originate from a single hadron is required to exceed 0.001. The invariant mass of $\pi^\pm\pi^0$ system must be in the range 0.45-1.20 GeV. In order to reject background from $\mathrm{Z} \to \mathrm{e^+e^-}(\gamma)$ and $\mathrm{Z} \to \mu^+\mu^-(\gamma)$, events with an electron or a muon candidate on the opposite side are rejected if its energy is grater then 42 GeV or can not be reliably measured.

The efficiency of the selection is 70% in the barrel. Figure 6 shows the selection efficiency as a function of the two polarization sensitive variables θ^*_ρ, the decay angle of the ρ^- in the τ^- rest frame, and ψ^*_ρ, the decay angle of the π^- in the ρ^- rest frame. The background in the barrel is 10.2% from other τ decays, 0.3% from $\mathrm{Z} \to \mathrm{e^+e^-}(\gamma)$ and 0.4% from $\mathrm{Z} \to \mu^+\mu^-(\gamma)$.

5. Measurement of the polarization.

5.1 Fitting procedure.

For each τ decay channel, $\mathcal{P}_\tau$ is measured by obtaining the linear combination of the $h = +1/2$, $h = -1/2$ Monte Carlo and the non-τ background distributions which best fits the data. The polarization of the background from other τ decays is varied simultaneously with the polarization for the decay mode being fitted. The normalization of the background from $\mathrm{Z} \to \mathrm{e^+e^-}(\gamma)$ and $\mathrm{Z} \to \mu^+\mu^-(\gamma)$ is left as a free parameter in the fit for the $\tau^- \to \mathrm{e}^-\overline{\nu}_\mathrm{e}\nu_\tau$ and $\tau^- \to \mu^-\overline{\nu}_\mu\nu_\tau$ events and is fixed for $\tau^- \to \pi^-(\mathrm{K}^-)\nu_\tau$ and $\tau^- \to \rho^-\nu_\tau$ decays. The contribution of all other background sources (mainly from two photon reactions and cosmics) was estimated from the data itself and is fixed in the fit for all the channels. The energy spectra for selected electrons, muons and pions, used for the polarization measurement, are shown in figures 7 through 9, together with the best fit Monte Carlo distributions.

For the analysis of the decay mode $\tau^- \to \rho^-\nu_\tau$ we fit a 10×15 matrix in the parameter space of θ^*_ρ, the decay angle of the ρ^- in the τ^- rest frame, and ψ^*_ρ, the decay angle of the π^- in the ρ^- rest frame. The spectra of $\cos\psi^*_\rho$ in four slices of $\cos\theta^*_\rho$ for the selected events are shown in figure 10, together with the best fit Monte Carlo distributions.

5.2 Charge identification.

$\mathcal{P}_\tau(\cos\theta)$ is obtained by measuring the polarization in seven regions of $\cos\theta$. The angle θ is defined by the thrust axis of the event signed according to the event charge, where the event charge is the charge of the τ traveling into the $\cos\theta > 0$ hemisphere. For events with at least one $\tau^- \to \mu^-\overline{\nu}_\mu\nu_\tau$ decay, the event charge is unambiguosly assigned by the muon chambers. For events with no identified muons but exactly one track in each hemisphere the charge is defined by the sign of the difference of curvatures weighted by resolutions for the two TEC tracks:

$$ch_1 \equiv -ch_2 = sign\left[\frac{c_1}{\delta c_1} - \frac{c_2}{\delta c_2}\right], \tag{7}$$

where $c = 1/P_\mathrm{T}$ is the curvature of the track and $\delta c_{1,2}$ is the curvature resolution. For all other events the charge is not defined and these are used for the measurement of average polarization only.

The average charge confusion for τ's is determined as a function of energy and polar angle from the measured TEC resolution, and a correction for its effect on polarization is applied in each $\cos\theta$ bin. The average charge confusion at $P = 45$ GeV is found to be about 3% in the barrel. The corresponding numbers for an average $Z \to \tau^+\tau^-$ event are 1.2%. For more details, see [12].

5.3 Measurement of polarization using the acollinearity.

The acollinearity between the τ decay products is also used to measure $\mathcal{P}_\tau$. We use the 1993 data sample for this measurement. For the selected sample consisting of 2565 $\tau^- \to \pi^-(\mathrm{K}^-)\nu_\tau$ events recoiling against a one prong τ decay, the acollinearity, ε, is defined as $\varepsilon = \pi - \alpha_{12}$, where α_{12} is the angle between the π^- track and the charged track in the opposite event hemisphere. The fiducial volume is restricted to the region of polar angle $|\cos\theta| < 0.68$. The efficiency in the fiducial volume as a function of the acollinearity is plotted in figure 11. The efficiency of the selection is 69.3%. The background contributions are 9.7% from other τ decays, 1.7% from Bhabha events, 0.5% from dimuon events, 0.1% from two photon interactions and 0.2% from cosmics. The acollinearity spectrum is shown in figure 12, together with the best fit Monte Carlo distributions.

5.4 Fit for $\mathcal{A}_\tau$ and $\mathcal{A}_\mathrm{e}$.

$\mathcal{P}_\tau(\cos\theta)$ is obtained by measuring the polarization in seven regions of $\cos\theta$ separately for every decay channel. The sizes of these regions are chosen such that they all contain approximately the same number of events. $\mathcal{A}_\tau$ and $\mathcal{A}_\mathrm{e}$ are determined by a fit of Eqn. 2 to the $\mathcal{P}_\tau(\cos\theta)$ dependence. Since Eqn. 2 neglects radiative corrections, contributions from γ-exchange and γZ-interference, the measurements of $\mathcal{P}_\tau(\cos\theta)$ must be corrected. The analytical program ZFITTER [20] was used to calculate these corrections. Given $\mathcal{A}_\tau$ and $\mathcal{A}_\mathrm{e}$, ZFITTER calculates $\mathcal{P}_\tau(\cos\theta)$ taking into account initial and final state radiation and their interference to $\mathcal{O}(\alpha^2)$ as well as the small contributions from γ-exchange and γZ-interference. The corrections are determined separately for each $\cos\theta$ bin. As these corrections show strong $\sqrt{s}$ dependence they are calculated for each $\sqrt{s}$ point and then averaged weighted by the integrated luminosity at these points. The summary of the $\mathcal{A}_\tau$ and $\mathcal{A}_\mathrm{e}$ measurements is presented in Table 2.

Finally the measurements of $\mathcal{P}_\tau(\cos\theta)$ for each individual τ decay mode are combined bin-by-bin in $\cos\theta$, taking into account the statistical correlation occuring when both τ decays are selected. Our estimate of the systematic errors is consistent with those obtained from the final analysis of 1993 data. The measured values of $\mathcal{P}_\tau$ for 1994, together with the corresponding corrections and statistical errors, and the systematic errors from 1993 are presented in Table 3.

$\mathcal{A}_\tau$ and $\mathcal{A}_\mathrm{e}$ are then determined by fitting Eqn. 2 to the corrected $\mathcal{P}_\tau$ values:

$$\begin{aligned}\mathcal{A}_\tau &= 0.156 \pm 0.017 \pm 0.008 \\ \mathcal{A}_\mathrm{e} &= 0.155 \pm 0.025 \pm 0.005.\end{aligned}$$

Here we have included a 3% correlation in our combination of the separate channels. The correlation coefficient between $\mathcal{A}_\tau$ and $\mathcal{A}_\mathrm{e}$ in the fit is $+0.030$. Fitting Eqn. 2 assuming $\mathcal{A}_\tau = \mathcal{A}_\mathrm{e}$ we obtain

$$\mathcal{A}_{\mathrm{e}-\tau} = 0.156 \pm 0.014 \pm 0.005.$$

The corrected $\mathcal{P}_\tau$ points together with the best fit curves are shown in figure 13. The systematic errors are obtained by propogating the bin-by-bin systematics in table 3 through to the final result as described in [14].

6. Conclusions.

From the measurement of $\mathcal{A}_\tau$ and $\mathcal{A}_e$ and our previous measurments [14], we derive the ratio of vector to axial-vector weak neutral couplings for electrons and taus:

$$
\begin{aligned}
g_V^e/g_A^e &= 0.0787 \pm 0.0078 \pm 0.0025 \\
g_V^\tau/g_A^\tau &= 0.0763 \pm 0.0051 \pm 0.0044.
\end{aligned}
$$

It agrees with other measurements of $\mathcal{P}_\tau$ performed at LEP [21–23].

Assuming lepton universality we derive the ratio of vector to axial-vector weak neutral couplings for leptons and the effective electroweak mixing angle:

$$
\begin{aligned}
g_V/g_A &= 0.0770 \pm 0.0043 \pm 0.0031 \\
\sin^2\theta_w^{\mathrm{eff}} &= 0.2308 \pm 0.0013.
\end{aligned}
$$

This is consistent with other L3 measurements of $\sin^2\theta_w^{\mathrm{eff}}$ extracted from the study of the Z lineshape and forward-backward charge asymmetries in the processes $Z \to b\bar{b}$, $Z \to e^+e^-(\gamma)$, $Z \to \mu^+\mu^-(\gamma)$ and $Z \to \tau^+\tau^-(\gamma)$ [24,25].

Table 2: $\mathcal{A}_e$ and $\mathcal{A}_\tau$ for each channel measured during 1991-1994 running periods. The errors correspond to data and Monte Carlo statistics. The quoted errors do not take into account statistical correlations arising when both event hemispheres are used for the fit.

Channel	1991/92 data	1993 data	1994 data
Measurement of $\mathcal{A}_\tau$:			
$e^-\bar{\nu}_e\nu_\tau$	0.119 ± 0.065	0.086 ± 0.079	0.129 ± 0.061
$\mu^-\bar{\nu}_\mu\nu_\tau$	0.182 ± 0.060	0.145 ± 0.074	0.115 ± 0.054
$\pi^-\nu_\tau$	0.141 ± 0.029	0.152 ± 0.036	0.163 ± 0.034
$\rho^-\nu_\tau$	0.161 ± 0.023	0.140 ± 0.028	0.168 ± 0.024
acollinearity	0.114 ± 0.065	0.103 ± 0.092	
Measurement of $\mathcal{A}_e$:			
$e^-\bar{\nu}_e\nu_\tau$	0.277 ± 0.090	0.203 ± 0.129	0.311 ± 0.089
$\mu^-\bar{\nu}_\mu\nu_\tau$	0.230 ± 0.083	0.210 ± 0.100	0.166 ± 0.078
$\pi^-\nu_\tau$	0.097 ± 0.045	0.177 ± 0.056	0.102 ± 0.049
$\rho^-\nu_\tau$	0.154 ± 0.036	0.145 ± 0.043	0.154 ± 0.036
acollinearity	0.135 ± 0.098	0.066 ± 0.130	

Table 3: The combined dependence of $\mathcal{P}_\tau$ on polar angle. $\delta\mathcal{P}_\tau^{\mathrm{QED}}$ represents a correction to $\mathcal{P}_\tau$ due to initial and final state radiation, γ-exchange and γZ-interference.

$\cos\theta$ range	$\mathcal{P}_\tau$	$\delta\mathcal{P}_\tau^{\mathrm{QED}}$	$\Delta\mathcal{P}_\tau^{\mathrm{stat}}$	$\Delta\mathcal{P}_\tau^{\mathrm{sel}}$	$\Delta\mathcal{P}_\tau^{\mathrm{bg}}$	$\Delta\mathcal{P}_\tau^{\mathrm{cal}}$	$\Delta\mathcal{P}_\tau^{\mathrm{chrg}}$	$\Delta\mathcal{P}_\tau^{\mathrm{theor}}$
$[-0.72, -0.55]$	-0.021	$+0.0000$	0.044	0.0045	0.0042	0.0126	0.0021	0.0007
$[-0.55, -0.35]$	-0.010	-0.0004	0.043	0.0045	0.0042	0.0128	0.0021	0.0007
$[-0.35, -0.12]$	-0.109	-0.0006	0.044	0.0046	0.0043	0.0129	0.0015	0.0007
$[-0.12, +0.12]$	-0.192	-0.0010	0.045	0.0048	0.0038	0.0137	0.0000	0.0007
$[+0.12, +0.35]$	-0.173	-0.0014	0.044	0.0046	0.0040	0.0127	0.0015	0.0007
$[+0.35, +0.55]$	-0.289	-0.0017	0.041	0.0045	0.0042	0.0128	0.0021	0.0007
$[+0.55, +0.72]$	-0.281	-0.0018	0.040	0.0045	0.0045	0.0130	0.0021	0.0007

References

[1] S. Jadach, Z. Was *et al.* in "Z Physics at LEP1", CERN Report CERN-89-08, eds. G. Altarelli, R. Kleiss and C. Verzegnassi (CERN, Geneva, 1989) Vol. 1, p. 235.

[2] S.L. Glashow, *Nucl. Phys.* **22** (1961) 579;
S. Weinberg, *Phys. Rev. Lett.* **19** (1967) 1264;
A. Salam, Elementary Particle Theory, Ed. N. Svartholm, Stockholm, "Almquist and Wiksell" (1968), 367.

[3] ARGUS Collaboration, H. Albrecht *et al.*, *Phys. Lett.* **B250** (1990) 164.
ARGUS Collaboration, H. Albrecht *et al.*, *Z. Phys.* **C58** (1993) 61.

[4] ARGUS Collaboration, H. Albrecht *et al.*, *Phys. Lett.* **B246** (1990) 278.
ARGUS Collaboration, H. Albrecht *et al.*, *Phys. Lett.* **B316** (1993) 608.

[5] ARGUS Collab., H. Albrecht et al., Phys. Lett. B341 (1995) 441.
ARGUS Collab., H.Albrecht et al., Phys. Lett. B349 (1995) 576.

[6] ALEPH Collab., D. Busculic et al., Phys. Lett. B346 (1995) 379.

[7] J.Gerald, P.Kapinos, W.Lohmann, R.Moore, "A measurement of the Michel parameters and the chirality parameter in $e^+e^- \rightarrow \tau^+\tau^-$ with the L3 Detector at LEP" *L3 Note 1792*, 1995.

[8] Y. S. Tsai, *Phys. Rev.* **D4** (1971) 2821.

[9] K. Hagiwara, A. D. Martin, D. Zeppenfeld, *Phys. Lett.* **B235** (1990) 198.

[10] A. Rougé, *Z. Phys.* **C48** (1990) 75.

[11] R. Alemany *et al.*, *Nucl. Phys.* **B379** (1992) 3.

[12] O. Adriani *et al.*, " A Measrement of τ Polarization",L3 Note 1637 (1994).

[13] S. Kirsch, "Neutral Current Physics with τ Leptons using the L3 Detector at LEP", PhD Thesis, Internal Report DESY-Zeuthen 94-04

[14] L3 Collaboration, M.Acciarri *et al.*, *Phys. Lett.* **B341** (1994) 245.
L3 Collaboration, O.Adriani *et al.*, *Phys. Lett.* **B294** (1992) 466.

[15] L3 Collaboration, B. Adeva *et al.*, *Nucl. Instr. and Meth.* **A289** (1990) 35;
O. Adriani *et al.*, *Nucl. Instr. and Meth.* **A302** (1991) 53;
K. Deiters *et al.*, *Nucl. Instr. and Meth.* **A323** (1992) 162;
J. A. Bakken, *Nucl. Instr. and Meth.* **A275** (1989) 81.

[16] S. Jadach, B.F.L. Ward and Z. Was, *Comput. Phys. Commun.* **66** (1991) 276;
R. Kleiss *et al.*, in "Z Physics at LEP1", CERN Report CERN 89-08 (1989), Vol. 3, p. 1.

[17] R. Brun *et al.*, "GEANT 3", CERN DD/EE/84-1 (Revised), September 1987.

[18] H. Fesefeldt, RWTH Aachen Preprint PITHA 85/02 (1985).

[19] T. Sjöstrand and M. Bengtsson, *Comput. Phys. Commun.* **43** (1987) 367;
T. Sjöstrand *et al.*, in "Z Physics at LEP1", CERN Report CERN 89-08 (1989), Vol. 3, p. 143.

[20] D. Bardin et al., FORTRAN package ZFITTER; CERN-TH 6443/92; *Z. Phys.* **C 44** (1989) 493; *Nucl. Phys.* **B 351** (1991) 1; *Phys. Lett.* **B 255** (1991) 290.

[21] ALEPH Collaboration, D. Buskulic *et al.*, *Z. Phys.* **C59** (1993) 369.

[22] DELPHI Collaboration, P. Abreu *et al.*, *Z. Phys.* **C55** (1992) 555.

[23] OPAL Collaboration, R. Akers *et al., Z, Phys.* **C56** (1995) 1.
G. Alexander, *et al.*, *Phys. Lett.* **B266** (1991) 201.

[24] L3 Collaboration, M. Acciarri *et al.*, *Z. Phys.* **C62** (1994) 551.

[25] L3 Collaboration, M. Acciarri *et al., Phys. Lett.* **B335** (1994) 542.

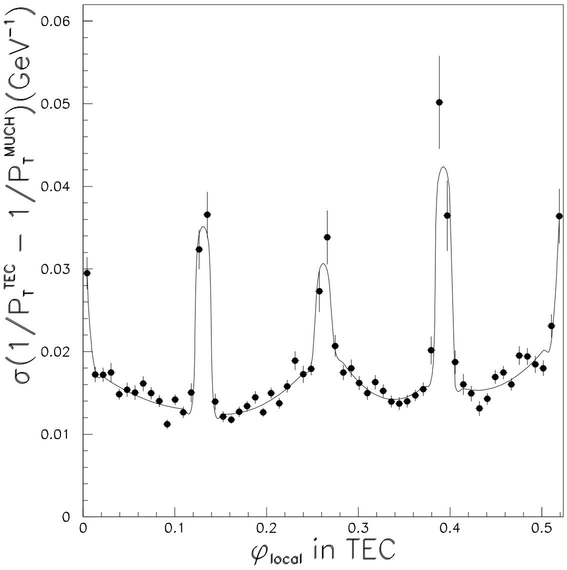

Figure 1: TEC resolution in the barrel region as a function of ϕ_{local} as determined from a comparison to muons in 1994 data. The average value is 0.015 GeV^{-1}.

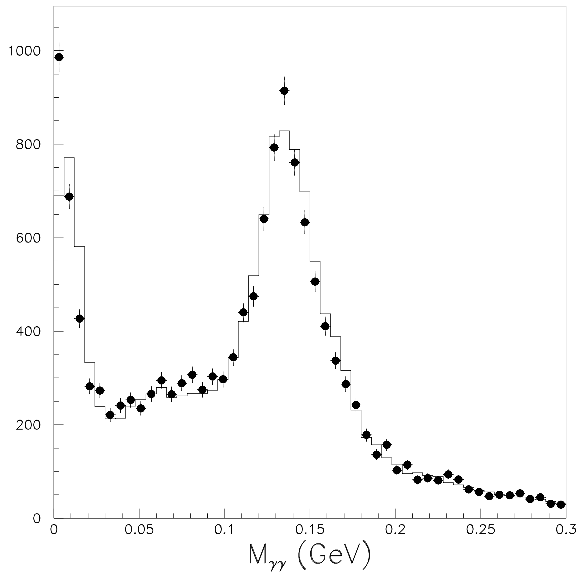

Figure 2: Reconstructed $M_{\gamma\gamma}$ from selected ρ decays. Included are events in which the two photons formed a single BGO bump.

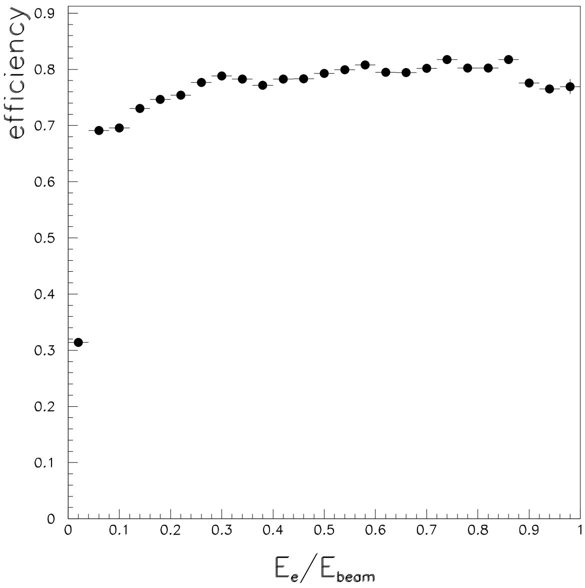

Figure 3: Selection efficiency of $\tau^- \rightarrow e^-\bar{\nu}_e\nu_\tau$ as a function of E_e/E_{beam} in the barrel region.

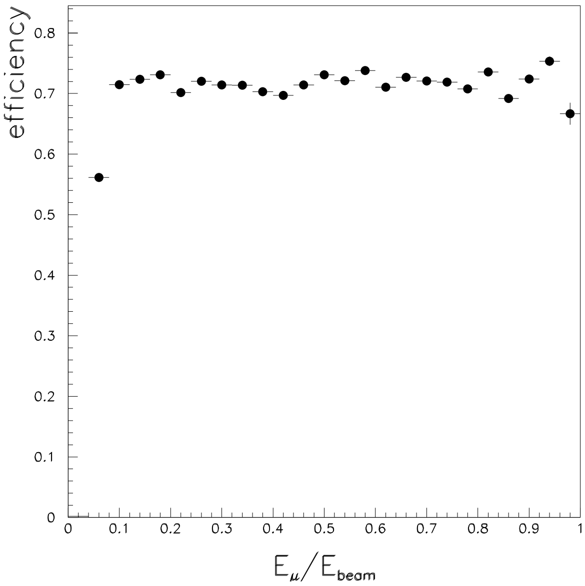

Figure 4: Selection efficiency of $\tau^- \rightarrow \mu^-\bar{\nu}_\mu\nu_\tau$ as a function of E_μ/E_{beam} in the barrel region.

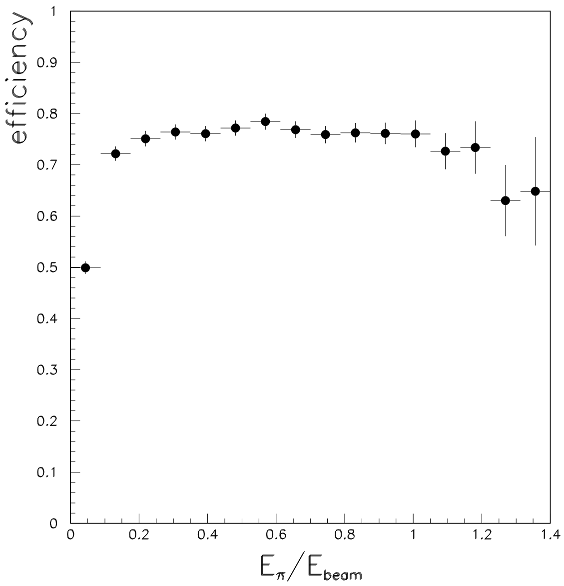

Figure 5: Selection efficiency of $\tau^- \to \pi^-(\mathrm{K}^-)\nu_\tau$ as a function of E_π/E_{beam} in the barrel region.

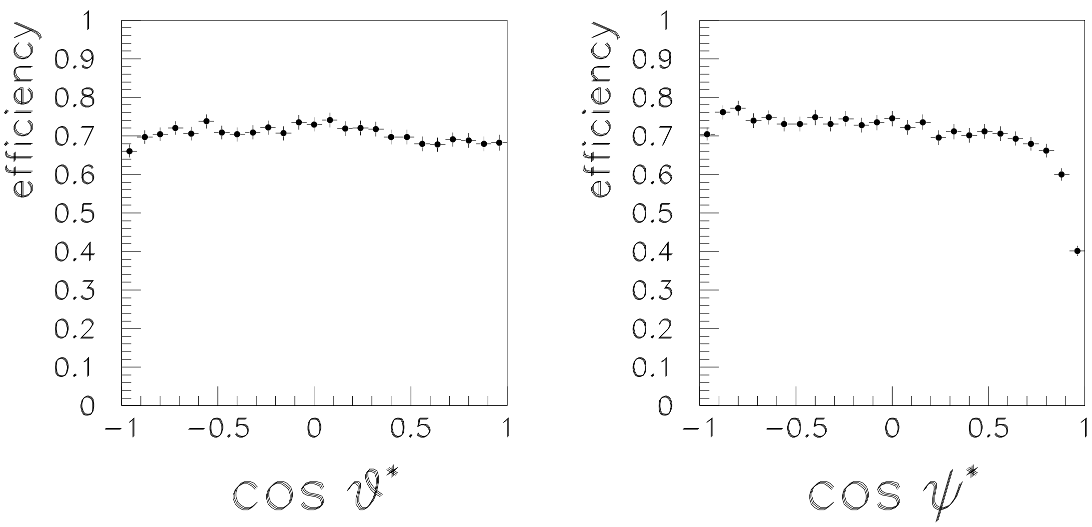

Figure 6: Selection efficiency for $\tau^- \to \rho^-\nu_\tau$ decays as a function of cos θ^*_ρ and cos ψ^*_ρ. cos θ^*_ρ is proportional to the sum of π^- and π^0 energies. cos ψ^*_ρ is proportional to the difference of π^- and π^0 energies.

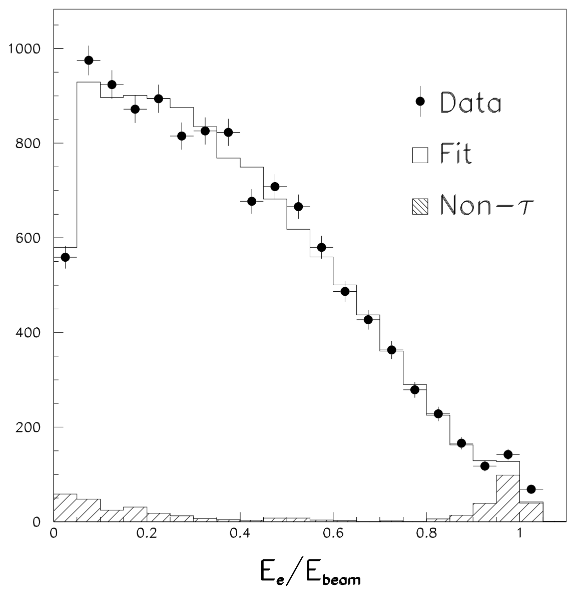

Figure 7: Spectrum for $\tau^- \to e^- \bar{\nu}_e \nu_\tau$ decays as a function of E_e/E_{beam}.

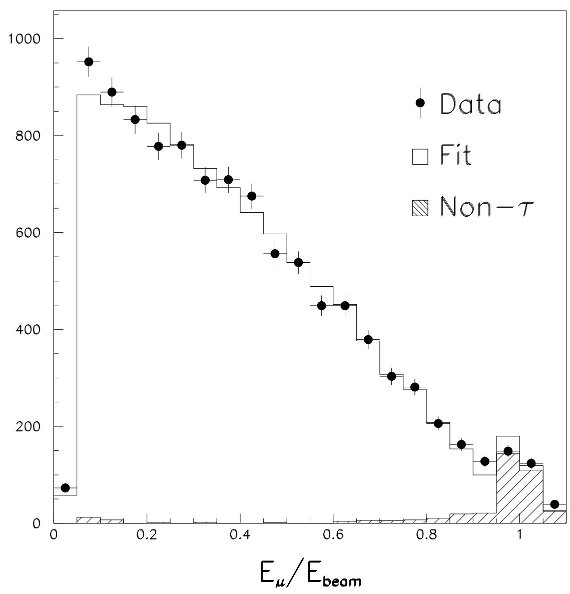

Figure 8: Spectrum for $\tau^- \to \mu^- \bar{\nu}_\mu \nu_\tau$ decays as a function of E_μ/E_{beam}.

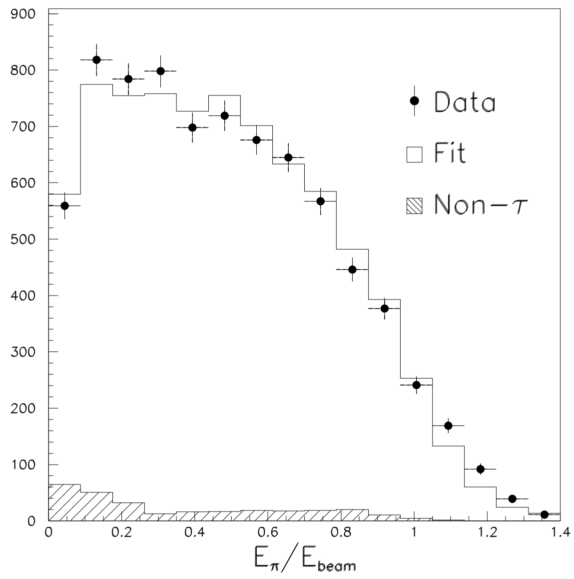

Figure 9: Spectrum for $\tau^- \to \pi^-(\mathrm{K}^-)\nu_\tau$ decays as a function of E_π/E_{beam}.

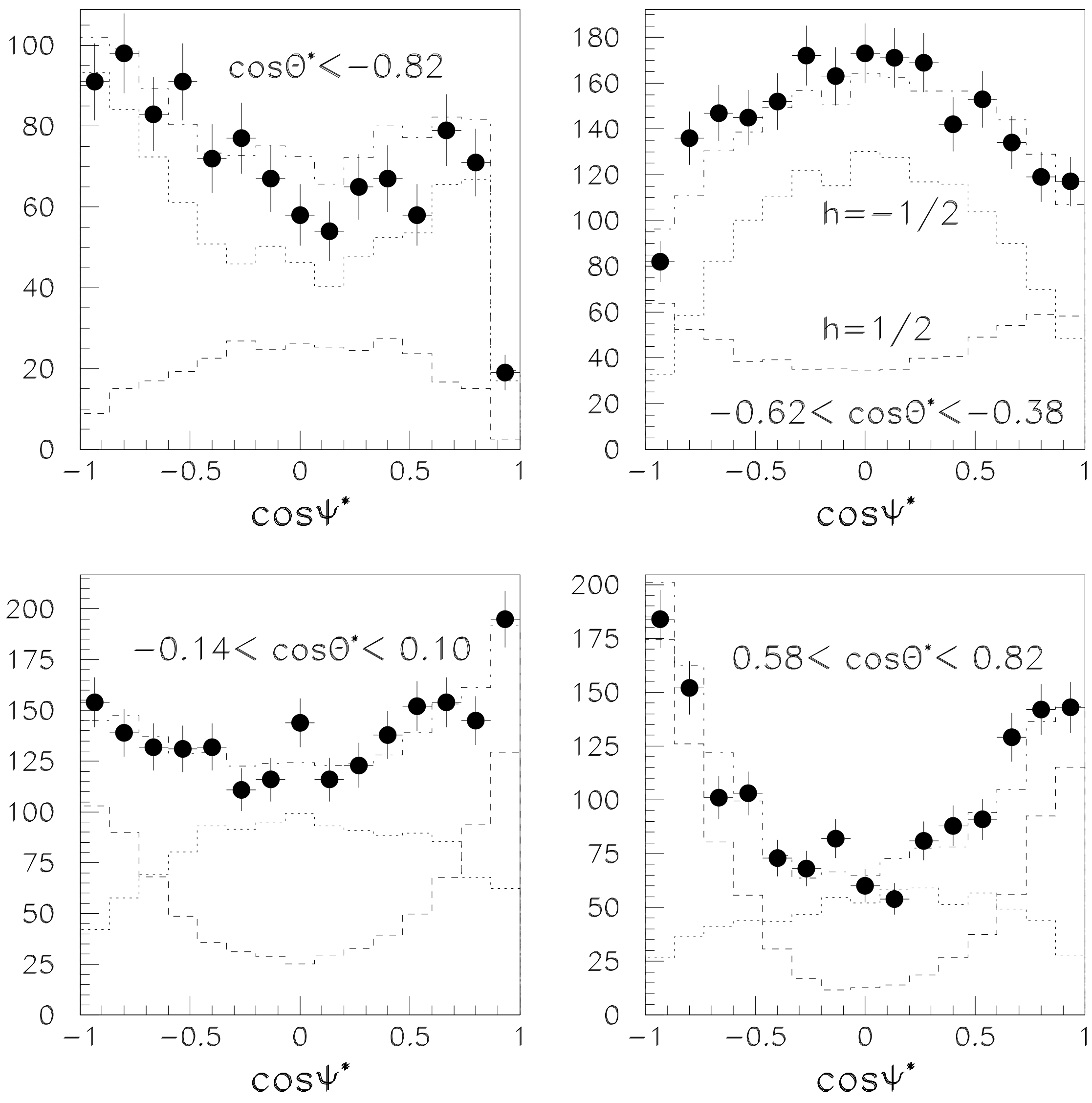

Figure 10: The spectra for $\tau^- \rightarrow \rho^- \nu_\tau$ as a function of cos ψ^*_ρ in four ranges of cos θ^*_ρ. Also shown are the Monte Carlo best fit, the contribution from each helicity. The ranges of cos θ^*_ρ are chosen to bring out the features of cos ψ^*_ρ distributions which provide the distingushing power for decays of τ^- leptons with positive and negative helicity states.

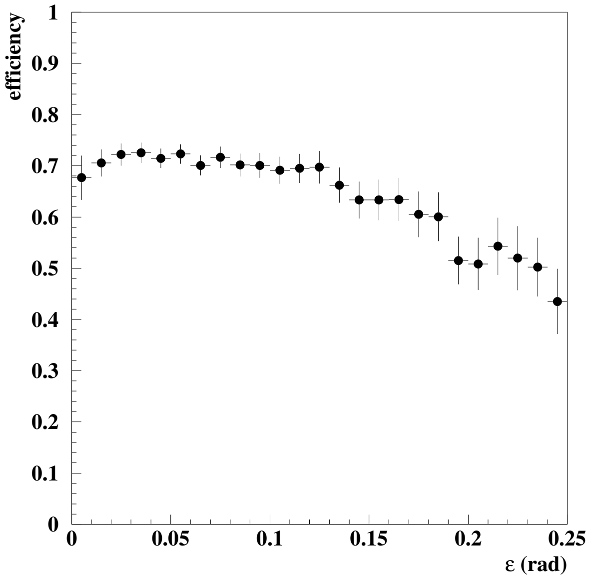

Figure 11: Selection efficiency for $\tau^- \to \pi^-(\mathrm{K}^-)\nu_\tau$ decays as a function of acollinearity, ε. The drop of the efficiency in the region of high acollinearity values is due to selection inefficiency at low E_{π^-}.

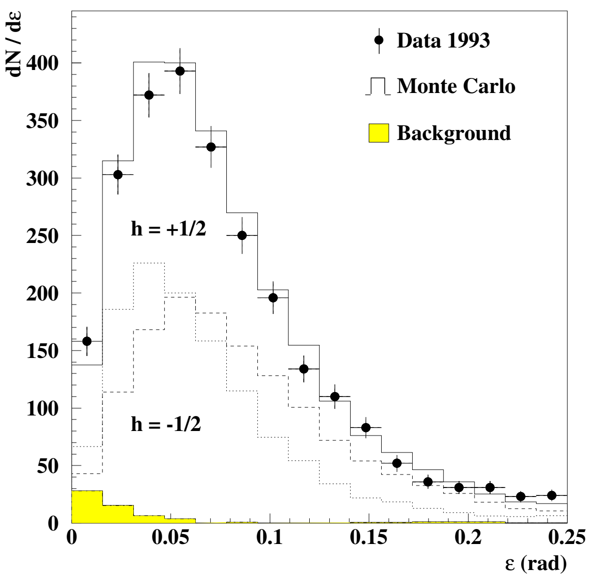

Figure 12: Spectrum for $\tau^- \to \pi^-\nu_\tau$ decays as a function of ε showing the Monte Carlo best fit, the contribution from each helicity, and non-τ background.

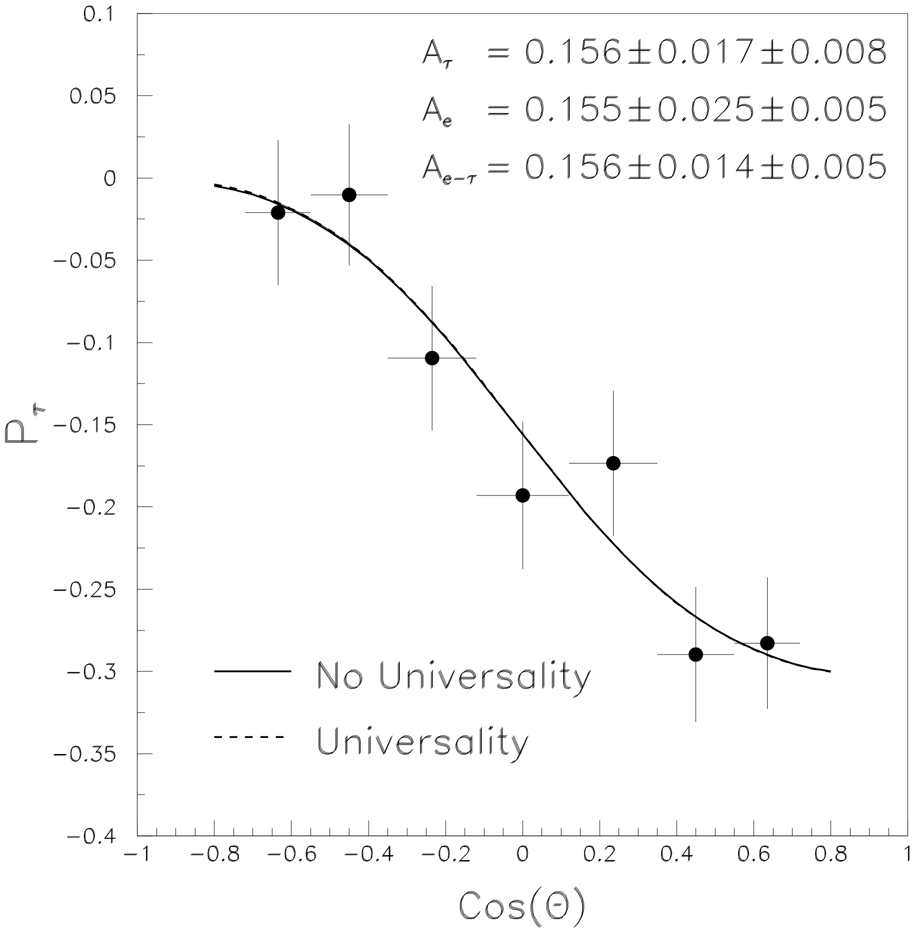

Figure 13: $\mathcal{P}_{\tau}$-$(\cos\theta)$ for the 1994 data with all channels combined, together with the fitted curves for $\mathcal{A}_\tau$, $\mathcal{A}_{\rm e}$, and for $\mathcal{A}_{{\rm e}-\tau}$ assuming $e-\tau$ universality. The errors include data, Monte Carlo statistics, and systematics. $\mathcal{P}_{\tau}$-$(\cos\theta)$ is corrected bin-by-bin for radiative corrections, γ-exchange and γZ-interference.